Direct-ink-writing (DIW) 3D printing functional composite materials based on supra-molecular interaction

Guiyan Yang[1], Youyi Sun[1*], Limin qin[1], Mengru Li[1], Kangtai Ou[1], Jiang Fang[1], Qiang Fu[1, 2*],

1.Shanxi Province Key Laboratory of Functional Nanocomposites, North University of China, Taiyuan 030051, P.R. China.

2.School of Civil and Environmental Engineering, University of Technology Sydney, Ultimo NSW 2007, Australia.

Abstract: Direct ink writing (DIW) is the most versatile AM technique in terms of materials development, it enables the creation of complex 3D shapes using any material by formulating a paste with controlled rheology. One of the main challenges of DIW is to design and formulate the viscoplastic and self-healing soft inks that easily flow under shear and quickly recover upon deposition. Researchers often look for flexible approaches that can be adapted to formulate printing inks with a wide range of materials. Here we report a supra-molecular interaction system composed of triethanolamine and ammonium oleate for application in DIW technology. Almost any materials (eg. rubber, plastic, ceramic, metal and composites) can be integrated into the ink system, and then can be 3D printing via shear-thinning DIW method. Furthermore, the solid contents of the ink system are higher than 80%, avoiding the formation of porous structure and dimensional changes after shaping. Present DIW method was used to construct sensors based on multi-material for application in real-time monitoring human health. This work may provide an new method to develop 3D printing materials for various practical applications.

Keywords: 3D Printing, DIW, functional, multi, supra-molecular.

Responding author: Fax: 86-351-3559669

E-mail address: syyi@pku.edu.cn (YY Sun); qiang.fu@uts.edu.au (QF).

1.Introduction

Novel manufacturing techniques such as 3D printing (3D printing, also referred to as additive manufacturing) play a critical role in building a sustainable future [1]. 3D printing can reduce waste, energy consumption and production time by eliminating the need to assemble components [1]. It also enables the mass customization of complex devices. Now, various 3D printing technologies were used and reported, such as binder jetting[2], material jetting[3], vat photopolymerization[4], powder bed fusion[5], energy deposition[6] and sheet lamination[7], fused deposition modelling (FDM)[8-9], direct-ink-writing (DIW)[10] and so on. Among these technologies, Direct ink writing (DIW) is the most versatile AM technique due to be suitable for more materials [11], in which almost any material can be –constructed to complex 3D shapes by the technology, such as ceramic [12], polymer [13], metal [14] or composite (or multi-material) structures [15]. As well-known, the design and synthesis of ink materials are the most important role for DIW technology. The ink materials should exhibit high viscoelasticity before extrusion, meanwhile have good shear-thinning effect when passing through a small nozzle, and restore high viscoelasticity after deposition to achieve shape fidelity [16]. These characters strongly depend on its chemical structure and properties of compositions in inks materials [17]. There are lots of works reporting the formulation design and the the rheological properties of inks materials for DIW technology. Unfortunately, a number of functional or composite materials that have proven to be widely used in industries cannot apply in DIW technology. The result is attributed to that it is difficult to design and prepare the functional or composite inks materials with simultaneously good shear-thinning effect and high modulus. So far, there are only a few literatures reporting the 'truly' multi-material or composite structures [18]. In addition, the organic solvents or aqueous content of the ink materials is generally high, while solid contents are generally low for achieving a good shear-thinning property. As a result, it easily induces the micropores and dimensional changes for the DIW structure after drying, debinding and consolidation [19]. These problems restrict the practical application of DIW technology in industry, and so far, DIW technology has been mainly exploited in research labs for small scale fabrication.

Ammonium oleate (AO) as a surfactant has attracted lots of attentions because of its excellent hydrophilic-lipophilic balance [20]. Taking the advantage of this system, chemists have successfully developed stable fluids containing nanotubes, metal oxides or magnetic particles with tunable viscoelasticity and good shear-thinning effects [21]. In addition, the triethanolamine further enhanced surface interactions between solid particles and water, preventing the phase separation of water and solid content during the extrusion process [22].

These also provide an opportunity to build a non-Newtonian fluid based on triethanolamine (TEOA) and ammonium oleate (AO) that can withstand various materials, *i.e.* polymer, ceramic, metals and composites for the shear-thinning DIW process. Furthermore, the resulting 3D structures can overcome the shortages aforementioned, effectively maintain their shape fidelity and realize the designed functions. Another goal is to enables a combination of different materials into complex structures by using single extrusion nozzles.

Here, a supra-molecular system based on ammonium oleate and ammonia was developed, which showed tunable viscoelasticity and excellent shear-thinning effects for DIW technology. The inks prove to print multi-materials or functional 3D structures using a series of valuable materials which are not applicable in conventional DIW method, such as nature rubbers, Al metal and so on. As a result, we successfully prepared a series of functional 3D objectives (*i.e.* rubber composite devices and precision metal parts) with record high solid contents and less structural micro-voids compared to conventional 3DP technologies. After a post-printing, thermal cross-linking or high temperature sintering, the mechanical stability/strength of the resulting 3D structures were further enhanced. Therefore, this study opens a new avenue for the development of versatile ink systems, which in turn broadens the practical applications of DIW 3DP technology.

2. Experiments

2.1 Materials

Natural rubber latex with ammonia as stabilizer was purchased from Hainan Shengyuan Rubber Industry Co., Ltd (solid content: 39%). Oleic acid (OA) and Triethanolamine (TTA) were purchased from Tianjin Kaitong Chemical Reagent Co., Ltd. Fumed silica (SiO_2), aluminium powder (Al), alumina powder (Al_2O_3), Rhodamine B (RhB), poly(vinylidene fluoride) (PVDF) and epoxy resin (EP) were purchased from Aladdin. The 1-chloromethyl ether 3-butylimidazole and graphene were synthesised by ours.

2.2 Preparation of 3D printing inks with various compositions

(1) Ammonium oleate (AO) inks

The oleic acid and 5 mL ammonia (5%) were mixed under mechanically stirring at room temperature. The volume of oleic acid was controlled to 0~10 mL for gel formation. Finally, the bubble in gels was removed *via* centrifugation.

(2)Ammonium oleate/nature rubber (AO/NR) inks

0.6 g triethanolamine was added to 20.0g rubber latex (solid content of 39%) under mechanically stirring for one minute. Then curing systems (e.g. tetramethyl thiuram disulfide,

2-mercaptobenzothiazole, sulfur and ZnO) were added to above dispersion solution under mechanically stirring for 5 minutes. Finally, 1.0g of oleic acid was added to above mixing solution under mechanically stirring, forming shear-thinning gels. The bubbles in shear-thinning gels were removed by the centrifugation at 6000 rpm for 10 minutes. The total solid content was about 74.0%.

In a comparison, the AO/NR based composite inks was also prepared. Firstly, the mixing solution (0.6 g triethanolamine, 20.0g rubber latex and curing systems) was prepared by the above process. Secondly, 0.8 g silica particles were added to above mixing solution under mechanically stirring. 10.0g carbonyl iron (CI), 2.0g graphene (G) or 0.5 g Rhodamine B (RhB) was further added to above mixing solution. Finally, 1.0g oleic acid was added to above mixing solution, forming AO/NR/CI, AO/NR/G and AO/NR/RhB gels, respectively. The total solid content was about 78.0%.

(3) AO/Al_2O_3 inks

0.6g triethanolamine was added to 10.0g ammonia (5%) under mechanically stirring. 25.0g Al_2O_3 particles, 1.0g silica particles, 0.2g TiO_2 particles and 0.2g CaO were further added to above mixing solution. Finally, 2.5g oleic acid was added to above mixing solution, forming OAA/Al_2O_3 gels. The solid content was about 85.0%. The bubbles in shear-thinning gels were removed by the centrifugation method at 6000 rpm for 10 minutes.

(4) AO/PVDF inks

0.6 g triethanolamine was added to 10.0g ammonia (5%) under mechanically stirring. 1.3g silica particles and 13.0g PVDF particles were further added to above mixing solution. Finally, 2.5 g oleic acid was added to above mixing solution, forming shear-thinning AO/PVDF inks. In the mixture, the solid content was about 66%. The bubbles in shear-thinning gels were removed by the centrifugation method at 6000 rpm for 10 minutes.

(5) AO/EP inks

0.6g triethanolamine was added to 10.0g ammonia (5%) under mechanically stirring. 1.3g silica particles and 13g EP particles were further added to above mixing solution. Finally, 2.5g oleic acid was added to above mixing solution, forming shear-thinning gels. The solid content was about 66%. The bubbles in shear-thinning gels were removed by the centrifugation method at 6000rpm for 10 minutes.

(6) AO/Al inks

0.6 g triethanolamine was added to 10g ammonia (5%) under mechanically stirring. 1.3 g silica particles and 20 g Al particles were added to above mixing solution. Finally, 2.5 g oleic acid was added to above mixing solution, forming shear-thinning gels. The bubbles in

the shear-thinning ink were removed by centrifugation at 6000 rpm for 10 minutes. The total solid content was about 80%.

2.3 DIW 3DP process based on a new new rotary-screw head

To print inks with high mechanical strength and high contents of solid particles, in this study, we designed a new rotary-screw head with 0.6mm nozzle as shown in Scheme 1A. The modified rotary-screw can provide larger mechanically shearing force, enhancing the shear thinning effect compared to conventional air press method. At the same time, a vacuum system was designed to prevent back-flow of printing ink.

This DIW 3DP process was conducted at room temperature. Various patterns were generated from the 3D software (CAD). Piezoresistive sensors were manufactured by placing printed core-shell components between copper electrodes as shown in Scheme 1B. The shell based on cross-linking CI/nature rubber (CI/NR) composite was firstly fabricated by DIW printing process and the core based on MR fluids suspension (Fe/CEBI) was continuously deposited in the pre-designed path.

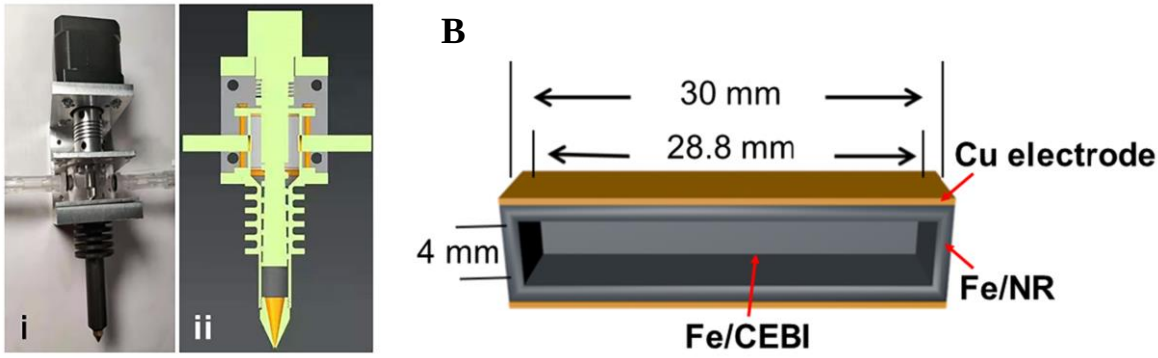

Scheme 1. (A)(i) optical photo and (ii) schematic diagram of present 3D printing nozzle based on screw extrusion. (B) the schematic diagram of present sensor by present DIW 3D printing.

2.4 Characterizations of DIW gels

The shear-thinning effect was characterized by a rheometer (MCR-302, Anton Paar, Austria) with a 20 mm flat plate device (1.0mm gap). Specifically, the steady-state mode with a shear rate of 0.01-1000s^{-1} was used for viscosity measurement. The storage modulus (G') and loss modulus (G") were measured at an oscillation mode with an angular frequency of 10 rad/s and a shear stress ranging 0 to 1000 Pa.

The microstructure and morphology of samples were characterized by Scanning electron microscope (SU-8010) at 5.0 kV acceleration voltage. Before characterizations, all the samples were immersed in liquid nitrogen and then fractured.

Fourier transform infrared (FT-IR) spectroscopy of samples was measured by FT-IR analyzer (FTIR-8400s) at 4000~400cm^{-1}.

The X-ray diffraction (XRD) pattern of samples was recorded by X-ray diffractometer (DX-2700B). The XRD data were collected with Cu K α radiation at 40 kV and 30 Ma at an angle of 2θ=1~5°.

The mechanical properties of rectangular specimens (60mm×10mm×30mm) were measured by a multifunctional testing machine (AI-7000-SGD) at room temperature.

2.5 Piezoresistive performance of sensor

The real-time current response (I-T curve) measurement of the sensor under different pressures and compressive strains were characterized by ourselves setups as shown in Scheme 1A. The electrochemical workstation (CHI660E) was used to record the relative current changes. The sensor test was carried out under a constant voltage of 6.0V. Under a constant voltage, the sensor was attached to the surface of the test body to record its I-t curve.

The piezoresistive performance of sensor as function of strain was characterized as shown in Scheme 1B. The deformation (or thickness) of sensor was adjusted and obtained by deformation controller. At the same time, the changes of electrical signals were recorded by electrochemical workstation. The strain（ε）was calculated according to the formula (1).

$$\varepsilon = \frac{d_o - d}{d_o} \times 100\%$$

The d_0 and d are the thickness of sensor before and after loading force.

The piezoresistive performance of the sensor as a function of frequency was determined as shown in Scheme S1. The loading force of sensor results from the repulsive interaction between ‘N’ pole of two magnets, leading to a deformation of sensor. The frequency was controlled by tuning the speeds (100, 200, 300 and 500rpm), corresponding to different frequencies of 1.67, 3.33, 5.0 and 8.33Hz, respectively. At the same time, the electrochemical workstation recorded the electrical signal changes of the tachometer at different frequencies.

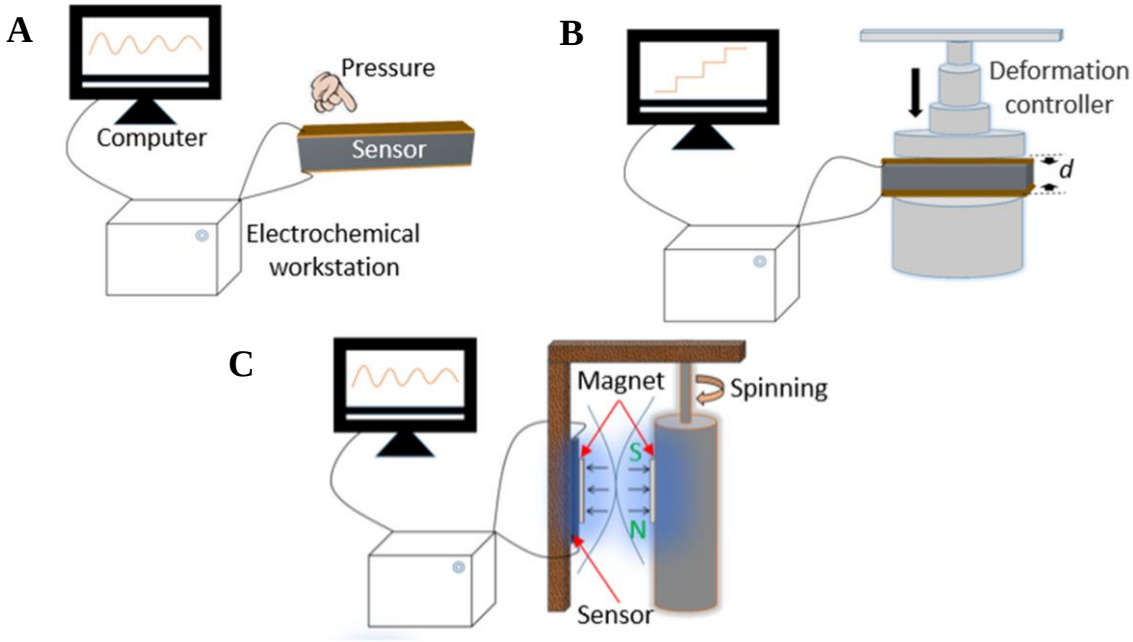

Scheme 2. Schematic illustration of the testing systems of sensors under (A) compressive force, (B) strains and (C) frequency.

3. Results and Results

In this study, we developed a novel shear-thinning gel system based on supra-molecular interaction between triethanolamine (TEOA) and ammonium oleate (AO) as a platform material, and then functional additives were introduced to produce DIW 3DP materials. Firstly, the molar ratio of oleic acid (OA) to $NH_3{\cdot}H_2O$ play a key role for the formation of shear-thinning gel system. Specifically, the mixture is liquid in the absence of OA or $NH_3{\cdot}H_2O$ (insert a-b of Fig.1A, and sFig.1A), and only when OA reaches a critical concentration of 0.3 mmol and the molar ratio of OA:$NH_3{\cdot}H_2O$ is higher than 7 (sFig.1B), the mixture can form a gel system as shown in inset c of Fig.1A. The micro-structure of the gel was further determined by the small angle x-ray diffraction (SWAXS, Fig.1A), polarizing optical microscope (inset d of Fig.1A) and IR spectra (Fig.1B). The XRD peak at 2.21^o indicated a typical highly ordered supra-molecular structure with a long period of 4.1 nm as shown in Fig.1A. In inset d of Fig.1A, we observed irregular texture and a large number of Maltese crosses, indicating the formation of liquid crystal structure in the obtained gels [23]. From the FT-IR spectra (Fig.1B), some characteristic absorption peaks at 2922.0cm^{-1}, 2850.0cm^{-1} and 1706.0cm^{-1} were observed, which were assigned to the C-H and C-O groups of OA, respectively. For the OA/$NH_3{\cdot}HO_2$ mixture, the peak assigned to C-O stretching became weak, indicating the formation of AO supra-molecular system by the H-bonding

between the carboxylic groups (-COO^-) of OA and the amino groups (-NH) of NH_3. For the OA/NH_3·HO_2/TEOA mixture, in addition to absorption peaks assigned to OA/NH_3·HO_2, a new absorption peak at 1024.0cm^{-1} was also observed, corresponding to C-N group of TEOA. Compared to pure TEOA (in sFig.1C), the absorption peak at 1024.0cm^{-1} was sharply reduced and the absorption peak at 882.0cm^{-1} assigned to H-N group of TEOA completely disappeared. The result indicated the formation of physical interaction between N-H of TEOA and carboxylic groups (-COO^-) of OA as shown in Fig.1C. Here, the lots of OH groups of TEOA were free, providing water retaining capacity of gels. The rheology properties of the AO and AO/TEOA gels were firstly evaluated as DIW inks as shown in sFig.2A. The viscosity of AO and AO/TEOA gels both sharply decreased from ~10^5 to ~10^3 mP·s with increasing in shear rate from 10^{-2} to 10^2 s^{-1}, indicating a good shear-thinning effect. The modulus vs stress of AO and AO/TEOA gels was further characterized as shown in sFig.2B. The storage modulus (G′) was clearly larger than loss modulus (G″), further indicating a AO and AO/TEOA gel character. In a comparison, the AO/TEOA gels showed better stability compared to AO gels, indicating a better printability. DIW printability of AO and AO/TEOA gels was further investigated and compared as shown in sFig.2C. For AO gels, the printing object was easily collapse and lose water, thereby clogging the nozzle of printer during the 3DP process. Contraily, the AO/TEOA gel displayed good structure stability and can retain water during 3DP process (sFig.2C-b). Based on the above results, a mechanism of formed AO/TEOA gel with good printability was proposed as shown in Fig.1C. Specifically, the formation of gel mainly relies on the highly ordered liquid crystal structure of AO and the H-bond between OA and water molecules. In addition, the incorporation of TEOA led to cross-linking between N^+ centre of TEOA and the COO^- groups of OA, further enhancing the mechanical stability of the gel-like inks. At the same time, the hydroxyl groups from TEOA would also interact with water molecules through H-bonding, thereby enhancing water retention capacity. These results indicated that the AO/TEOA gel exhibited good printability and water retention compared to single AO gel during the 3DP process.

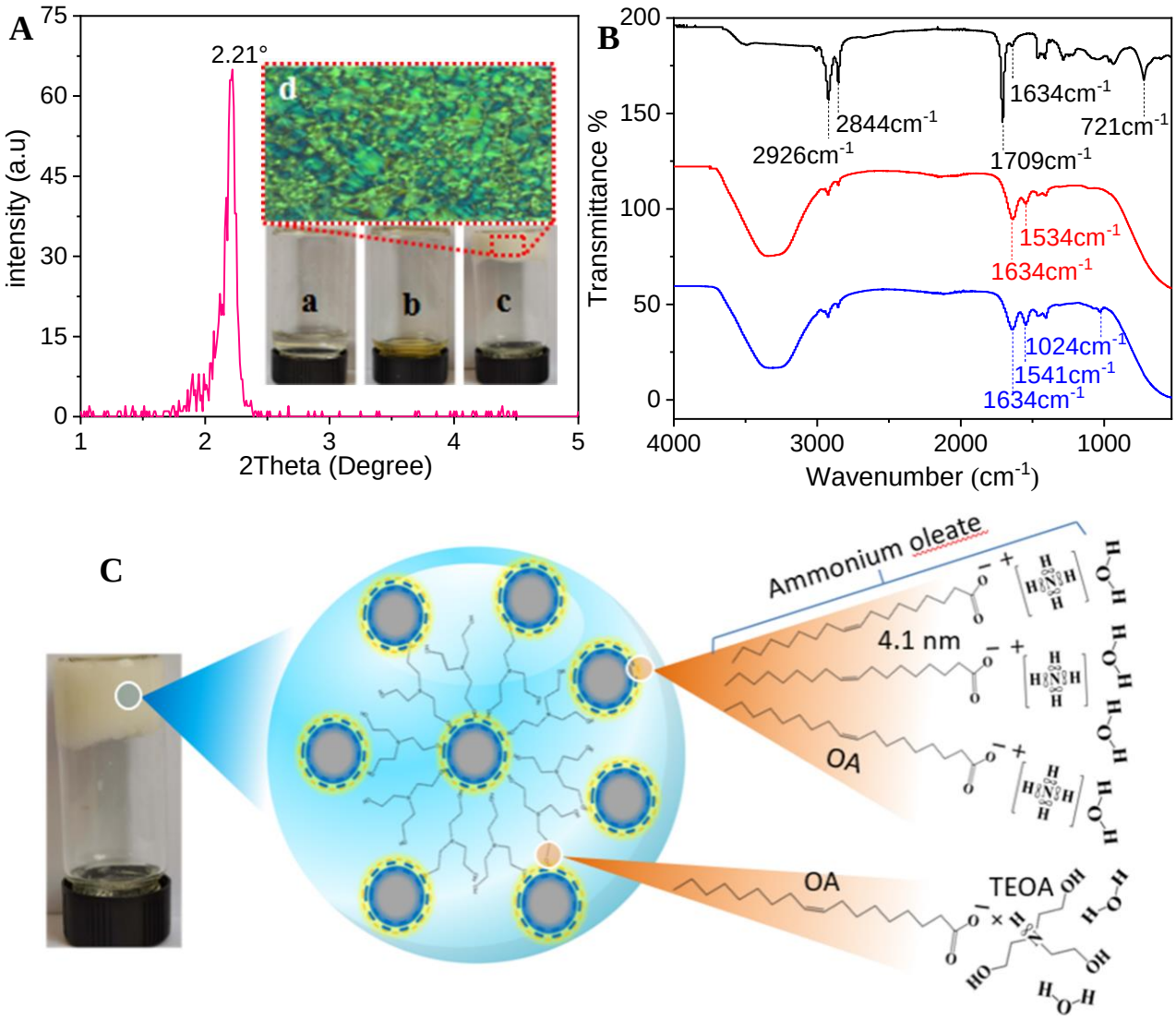

Fig.1. (A) SWAXS pattern of AO gel. Insets (a-c) are the optical photographs of OA, $NH_3{\cdot}H_2O$ and the AO gel, respectively. Inset (d) is the polarizing optical microscope of AO gel. (B) FT-IR spectra of (a) OA and (b) AO and AO/TEOA gel, (C) Schematic illustration of the formation of AO/TEOA gel based on supra-molecular interaction.

Based on the versatile AO/TEOA gel, a series of functional composite gels were designed and prepared, such as AO/TEOA/NR, AO/TEOA/NR/CI, AO/TEOA/NR/G and AO/TEOA/NR/RhB as shown in insets of Fig.2A. The rheological behavior of these functional composite gels were characterized as shown in Fig.2A. It was found that all additives were well dispersed in the AO/TEOA gel and were few effect on their shear-thinning properties. All functional composite gels exhibited a similar viscosity (η) of ~10^6 mPa·s at low shear rate of ~$0.01s^{-1}$. When increasing the shear rate from 0.01 to 1,000 s^{-1}, the η of all functional composite gels dramatically decreased from 10^6 to 10^2 Pa·s. Due to their strong shear-thinning effect, the obtained functional composite gels can also easily extrude

from the nozzle under shearing force, and then restore their high viscosity and form stable gel filaments. Fig.2B shows the G′ and G″ of all functional composite gels as a function of shear stress. It was found that the G′ was significantly higher than the G″, indicating a gelled structure, which facilitated high shape fidelity of the printed structures. At the crossover point between the two moduli curves, we observed a shear yield stress (τ_y) of ~90 Pa, indicating high stiffness and yield stress. As a result, these functional composite gels were ideally suited for DIW 3DP process. In addition, these additives (eg. SiO_2, CI, graphene, etc) were few aggregation or sedimentation –in AO/TEOA gel due to gel state, which was also crucial for DIW 3DP. It was also attributed to amphipathic molecule of OA and TEOA with functional groups, providing a good compatibility between water and other non-polar materials (NR, CI or graphene). These results indicate that AO and TEOA are not only key role for formation of DIW gels, but also play important role for preparation of various composite or functional DIW gels.

a

Fig.2. The curves of (A) viscosity *vs.* shear rate and (B) modulus *vs.* shear stress of (a)AO/TEOA/NR, (b)AO/TEOA/NR/SiO_2, (c)AO/TEOA/NR/SiO_2/graphene, (d)AO/TEOA/NR/SiO_2/CI, and (e)AO/TEOA/NR/SiO_2/RhB gels. The inserts are the optical images of corresponding gels.

The DIW printability of the functional composite gels was further evaluated as shown in Fig.3. Generally, the DIW 3DP process is divided into three steps, namely (i) extruding the ink to form filaments, (ii) depositing the filaments to form basic units, and (iii) stacking the filaments to produce 3D structures. Therefore, printability analysis was carried out according to the above three steps. As shown in Fig.3A, when the AO/TEOA/NR/SiO_2 inks are extruded through a 600μm nozzle, the ink can form a steady flow and the fluid immediately self-healed to form a stable and continuous gel filament. At the same time, the length of the

filament increases linearly during printing at a printing speed of 9.45 mm s^{-1}. This rapid printing speed was attributed to the high mechanical shear force through a screw extrusion, which could effectively enhance shear-thinning effect compared to conventional air pressure shear force. The content of AO/TEOA on printability of AO/TEOA/NR/SiO_2 inks was also

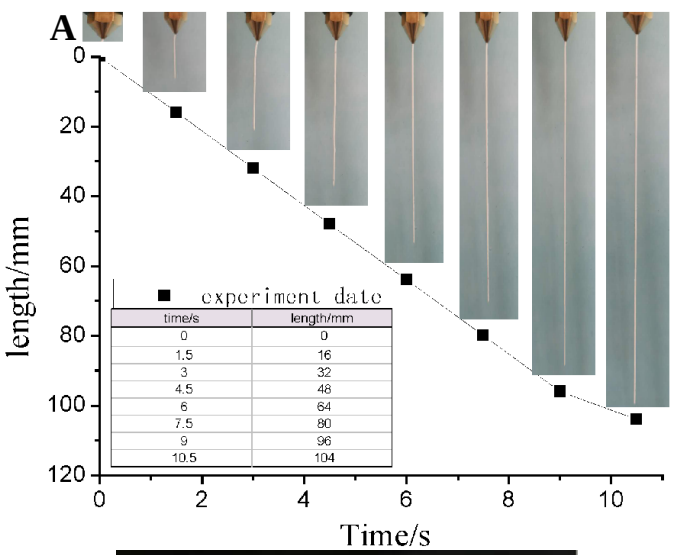

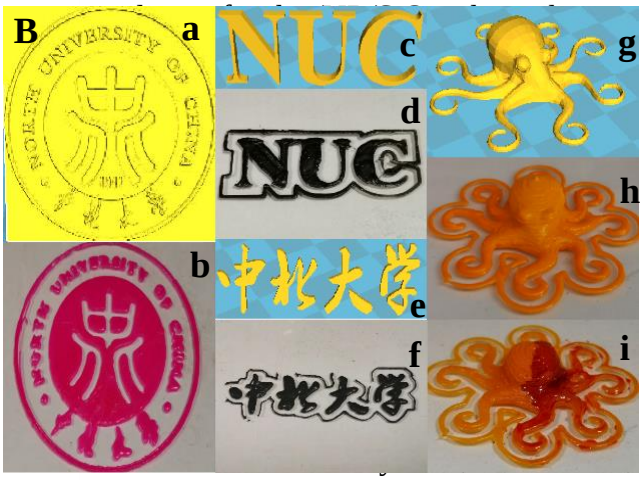

edical devices to aircraft due to good

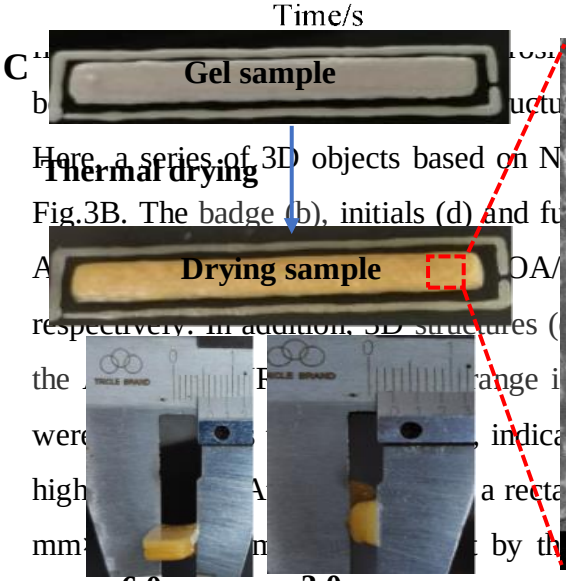

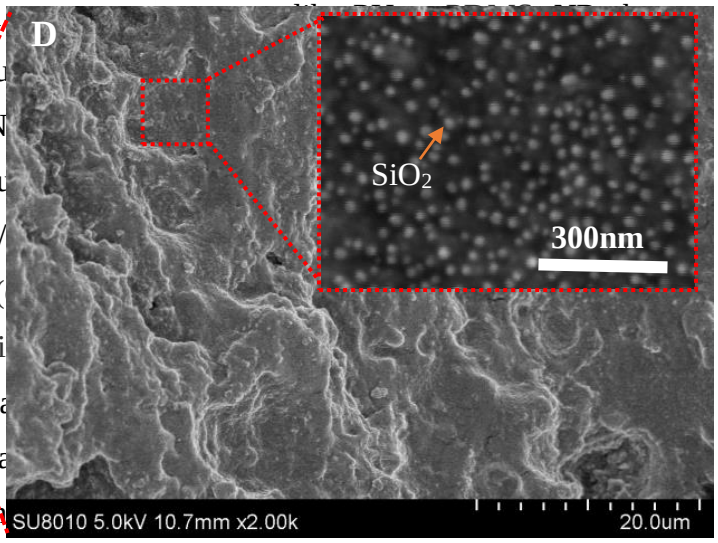

Here, a series of 3D objects based on N
Fig.3B. The badge (b), initials (d) and fu
A OA/
respectively. In addition, 3D structures (
the range i
were , indica
high A a recta
mm by th
(Fig.3C). Interestingly, the shape and size of the sample were almost identical before and after thermal drying, which was attributed to the high solid content of the printed object and the resulting compact structure (in Fig.3D). This unique thermal stability of 3D printing gel was rarely reported in previous studies [24-27]. In fact, 3D structures based on conventional DIW inks mostly shrank or broke after thermal drying due to their porous structure. In addition, we observed that the SiO_2 nanoparticles were evenly distributed in the matrix of the printed object, thereby enhancing the ability to resist shrinkage or deformation (Fig.3D). After thermal drying, the covalent cross-linking of NR and the chemical reactions between OA and SiO_2 would further enhance the mechanical and thermal stability of the obtained 3D object. All the factors discussed above make the present ink based on the AO/TEOA platform

to act as an ideal material for DIW 3DP to produce 3D structures with high shape fidelity, high mechanical/thermal stability and high-resolution.

Fig.3. (A) The optical photographs of the steady flow of AO/TEOA/NR/SiO_2 inks out of the nozzle. (B) The CAD models and printed 3D structures with varying geometry: (a-b) the badge, (c-d) initials and (e-f) full name of the North University of China, respectively, and (g-i) the octopuses. (C) The optical photographs of 3DP objects using AO/TEOA/NR/SiO_2 inks (a) before and (b) after thermal drying. (D) SEM images of the 3DP object after thermal drying.

The structure and property of 3DP objects based on NR were further investigated by XRD and IR measurements as shown in sFig.4A and 4B, respectively. A wild weak peak at 22.0^o was clearly observed for all samples, which was assigned to the amorphous NR component (in sFig.4A). In addition, a strong peak at 45.0^o was observed for 3DP object

using AO/TEOA/NR/SiO_2/CI inks, which was assigned to (110) pattern of Fe (JCPDS card No. 06-0696) [28]. Due to non-crystalline structure of graphene and RhB, no characteristics peak in XRD was observed. Both the pure NR latex and the obtained 3DP objects showed similar IR absorption peaks (sFig.4B). These results confirmed the successfully preparation of 3DP objects using various functional ink materials. In addition, micro-structure of 3DP objects was also characterized by SEM images as shown in sFig.5. All samples showed compact structure and no micropores were observed. Furthermore, the 3DP objects formed chemical cross-linking structure in presence of vulcanization ingredients after thermal treatment, which was confirmed by the equilibrium swelling method (sFig.6). The cross-linking density of all functional 3DP objects was higher than 1.2mol/cm^3. These results

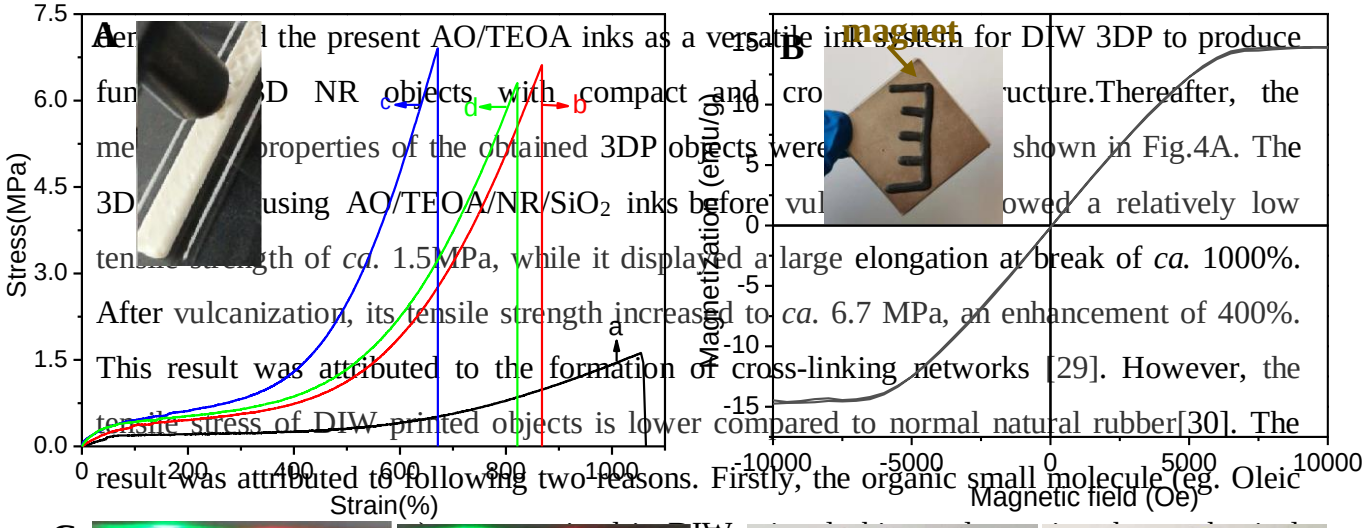

Aer l the present AO/TEOA inks as a versatile ink system for DIW 3DP to produce fun 3D NR objects with compact and cro ructure.Thereafter, the me roperties of the obtained 3DP objects were shown in Fig.4A. The 3D using AO/TEOA/NR/SiO_2 inks before vul owed a relatively low tens gth of *ca.* 1.5MPa, while it displayed a large elongation at break of *ca.* 1000%. After vulcanization, its tensile strength increased to *ca.* 6.7 MPa, an enhancement of 400%. This result was attributed to the formation of cross-linking networks [29]. However, the tensile stress of DIW-printed objects is lower compared to normal natural rubber[30]. The result was attributed to following two reasons. Firstly, the organic small molecule (eg. Oleic

mer
e in
/NR/
rcem

compared the mechanical properties of 3D objects produced using the present and previous inks (*e.g.* PU or PDMS) [13, 32-40]. As shown in sFig.7, the present 3DP object displayed a more excellent overall performance, especially the tensile strength. The M-H curve of the 3DP object using AO/TEOA/NR/SiO_2/CI inks was characterized in a magnetic field range of -11000 to +11000 Oe at 298K (Fig.4B). The magnetization intensity linearly responded to the applied magnetic field, indicating paramagnetic behaviour [41]. The magnetization saturation (MS) of the 3DP object was *ca.* 15.0 emu g^{-1}. This object can also be easily adsorbed on a magnet as shown in inset of Fig.4B. These results indicated formation of 3DP object with good magnetic property. The electric conductivity of 3DP objects using AO/TEOA/NR/SiO_2/G and AO/TEOA/NR/SiO_2/CI inks was determined to be 0.08 and

0.03 S/m, respectively, which was three orders of magnitude higher than pure nature rubber. After connecting the circuits, the LED lighted up, further indicating the high conductivity of the 3DP objects (Fig.4C). Furthermore, we found that the 3DP object using AO/TEOA/NR/SiO_2/RhB inks exhibited discoloration behaviour at different pHs. Its colour changed from orange to red in an acid solution (Fig.4D). These results revealed the advantages of the present AO/TEOA ink materials, allowing for the DIW 3DP to produce functional 3D structures for various applications, which was difficult to be realized by other 3DP process (e.g. FDM) using conventional rubber or elastomer inks.

Fig.4. (A) Tensile stress-strain of 3DP objects using (a) uncross-linked AO/TEOA/NR/SiO_2 inks, (b) cross-linked AO/TEOA/NR/SiO_2 inks, (c) cross-linked AO/TEOA/NR/SiO_2/G inks and (d) cross-linked AO/TEOA/NR/SiO_2/CI inks. (B) VSM curves of the 3D object using AO/TEOA/NR/SiO_2/CI ink. (C)Electrically conductive 3D objects using AO/TEOA/NR/SiO_2/G and AO/TEOA/NR/SiO_2/CI inks. (D) pH sensitive performance of the 3D object using AO/TEOA/NR/SiO_2/RhB inks. The inset of (A) is optical photo of cross-linked 3DP samples using AO/TEOA/NR/SiO_2 inks. The inset of (B) is optical photo of cross-linked 3DP samples using AO/TEOA/NR/SiO_2/CI inks in presence of magnet.

We then designed and produced a new class of piezoresistive sensors by DIW 3DP of the functional composite inks. The 3DP cuboid box using AO/TEOA/NR/SiO_2/CI inks mainly provided excellent elasticity and packaging for the sensor. At the same time, 3DP cuboid box using AO/TEOA/NR/SiO_2/CI inks showed simultaneously good magnetic

property and conductivity, which was key role for piezoresistive sensors. The sensing materials was magnetorheological fluids based on CI particles and magnetic ionic liquids (MIL). As shown in sFig.8A, different mechanical pressures (e.g. click, face and point) could induce different current responses. The current-time curves showed an asymmetric shape in response to the face and point pressures, while showed a linear shape in response to click pressure. As shown in sFig.8B, the current signal has a gradually increase trend, responding to the gradual increase in compression strains from 0 to 15%. Of particular note, the sensor showed excellent sensitivity with an ultra-low detection limit of 1.6% strain, which was rarely reported in previous studies[42-43]. In fact, conventional piezoresistive sensors could usually only respond to larger compression strains greater than 10%. In addition, a large strain was further applied to the sensor, and during each application of a specific compressive

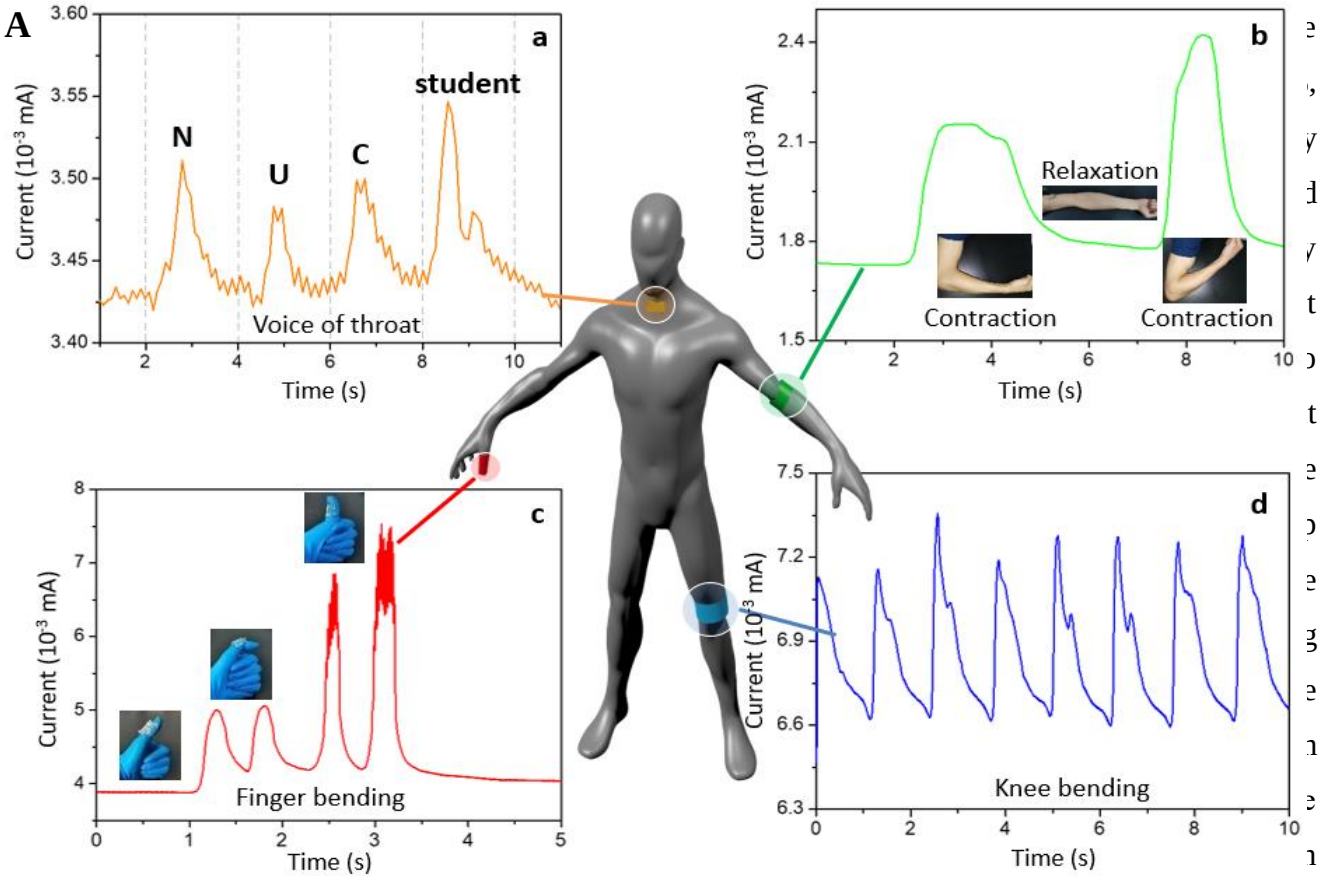

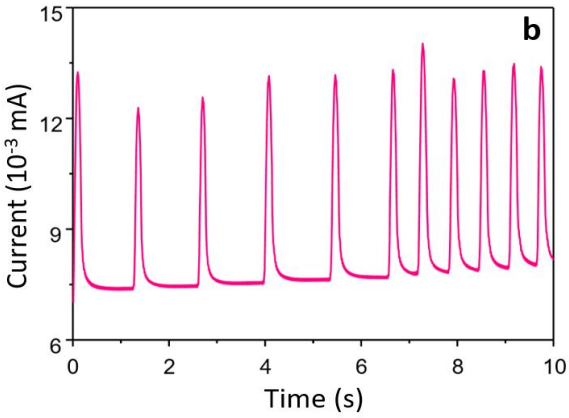

sensing applications. We fixed the sensor on the frame of a bicycle, meanwhile fixed a magnet on the spoke of its rear wheel (Fig.5B-a). When the wheel rotates, the distance between the magnet and the sensor alternately changes, leading to a alternate change of presuure. When the distance between the magnet and the sensor is the shortest, it provides a largest presuure, leading to a highest signal as shown in Fig.5B-b. It shows the change in relative resistance at the beginning of a ride. By counting the average and total number of peaks, we can easily track the speed and traveling distance of the bicycle. The non-contact sensing was attributed to the 3D printed magnetic shell of the sensor, which was composed of CI and NR.

Fig.5. (A) Real-time detectability of 3D printing sensor in monitoring activity of human: (a) throat, (b) arm, (c) finger and (d) knee joints. (B) Real-time detectability of the speed and

traveling distance of the bicycle: (a) the illustration of the reaction set-up and (b) the real-time current change of sensor under movement of bicycle.

In order to further highlight the universality of present AO/TEOA gels based on supra-molecular interaction, these composite gels (eg. AO/TEOA/PVDF, AO/TEOA/epoxy, AO/TEOA/Al_2O_3 and AO/TEOA/Al) were also prepared and investigated. All the components (eg.PVDF, epoxy, Al_2O_3 or Al particles) could be well dispersed in the AO/TEOA gels (sFig.9A). Moreover, it formed stable gel-like composite inks with good shear-thinning effect, which played a key role in the DIW 3DP process (sFig.9B). The leaf, butterfly and cuboid were designed by CAD software and then were produced by DIW 3D printing AO/TEOA/Al_2O_3/RhB, AO/TEOA/Al_2O_3/methylene red and AO/TEOA/Al_2O_3/G inks, respectively as shown in Fig.6A. These 3DP Al_2O_3 objects were difficult to be produced by conventional Laser sintering method due to mutil-material structure. The XRD pattern of 3DP Al_2O_3 objects were firstly characterized as shown in Fig.6B. The 3DP Al_2O_3 objects without and with graphene nanosheets both possessed some diffraction peaks at 2θ=25.8°, 35.5°, 38.1°, 43.6°, 52.8°, 57.7°, 61.5°, 66.8°, 68.5° and 77.1°, which were assigned to the (012), (104), (110), (113), (024), (116), (211), (214), (300) and (208) crystal planes of α-Al_2O_3 (JCPDS card No. 78-2426) [45], respectively. The formation of 3DP Al_2O_3 objects with graphene nanosheets was further confirmed by the Raman spectrum (in Fig.6C). It clearly showed two peaks at 1355.0cm^{-1} and 1594.0cm^{-1}, which were assigned to D and G

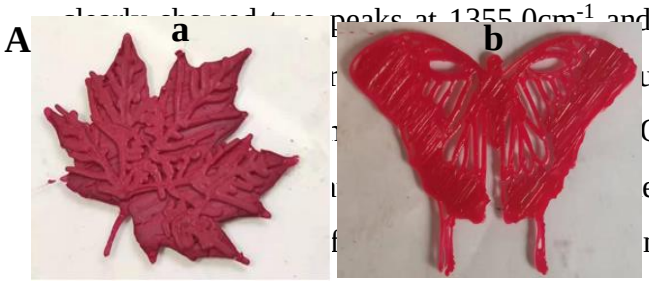

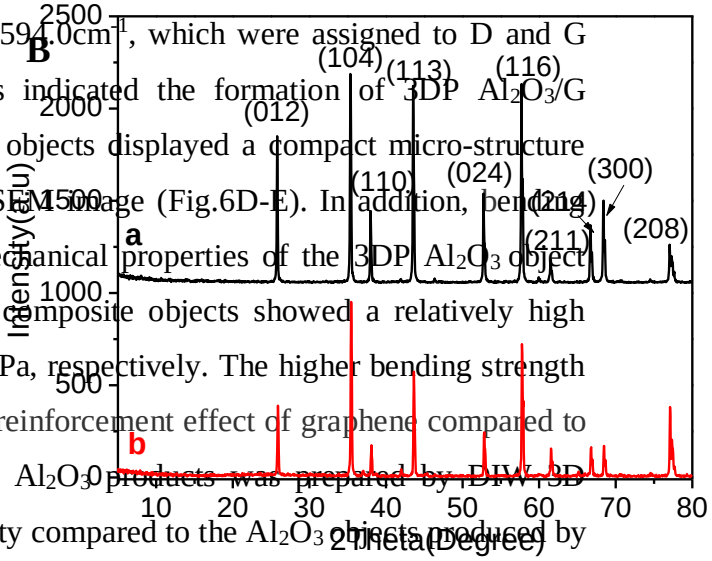

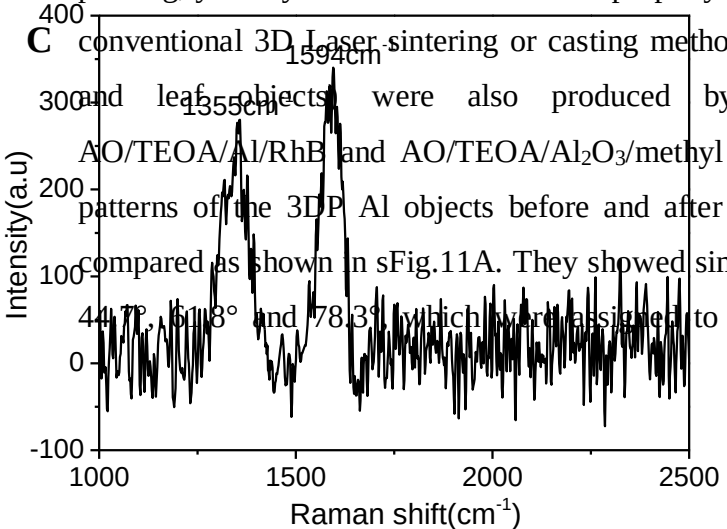

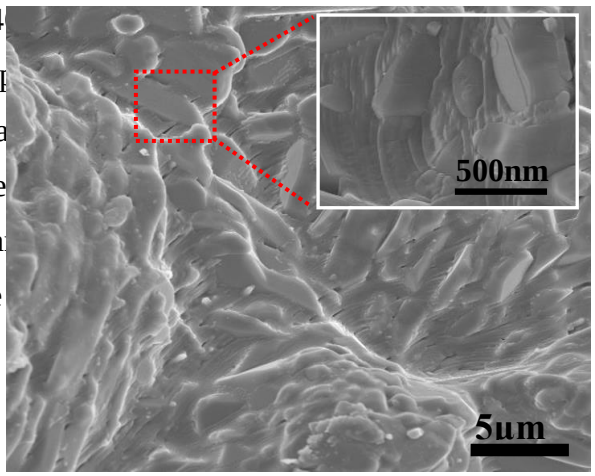

results indicated the formation of 3DP Al_2O_3/G ...O_3 objects displayed a compact micro-structure ...e SEM image (Fig.6D-E). In addition, bending ... mechanical properties of the 3DP Al_2O_3 object (Fig.6F). The 3DP Al_2O_3 object and Al_2O_3/G composite objects showed a relatively high ...5MPa and 214.7 MPa, respectively. The higher bending strength ...ts was attributed to reinforcement effect of graphene compared to 3DP Al_2O_3 object. Although the present 3DP Al_2O_3 products was prepared by DIW 3D printing, yet they had similar mechanical property compared to the Al_2O_3 objects produced by conventional 3D Laser sintering or casting method[4]. ... and leaf objects were also produced by ... AO/TEOA/Al/RhB and AO/TEOA/Al_2O_3/methyl ora... patterns of the 3DP Al objects before and after the ... compared as shown in sFig.11A. They showed simila... 44.7°, 65.0° and 78.3°, which were assigned to the

planes of Al (JCPDS card No. 89-4037), respectively [18]. The result indicated that the 3DP Al object was not oxide during 3D printing and thermal sintering process. The IR spectra of these 3DP objects based on AO/TEOA/EP/methyl orange and AO/TEOA/PVDF/RhB inks were also characterized and compared as shown in sFig.11B and sFig.11C, respectively. The characteristic absorption peaks of PVDF and EP were observed and were few changes before and after thermal dying. Furthermore, the micro-structure of these 3DP objects were also characterized by the SEM images (sFig.12A-C). All samples showed compact and non-porous structure. The mechanical strength was also evaluated as shown in sFig.13. It was found that these 3DP small rings could lift weight (>100g), indicating good mechanical strength. In a comparison, these inks without AO/TEOA system can not be 3D printed as shown in sFig.14. Although the mixture with Al_2O_3 and water solidified due to high content (78%), yet it was not gel state as shown in sFig.14B. At the same time, it also showed poor shear-thinning effect. So, it easily clogged the nozzle as shown in inset of sFig.14A. These results further demonstrated the versatility of the present AO/TEOA ink for DIW 3DP.

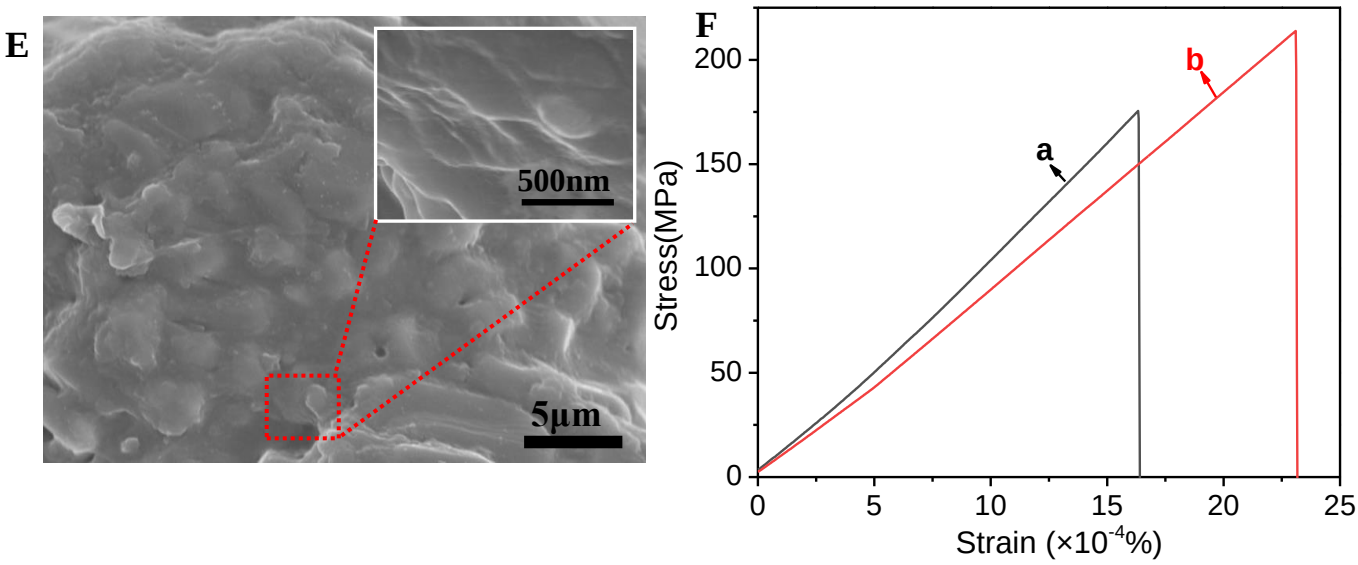

Fig.6. (A)Optical photograph of 3DP Al_2O_3 objects using (a) AO/TEOA/Al_2O_3/RhB, (b)AO/TEOA/Al_2O_3/GO/methylene red inks before sinter, (c)AO/TEOA/Al_2O_3 inks after sinter and (d)AO/TEOA/Al_2O_3AO/TEOA/GO inks after sinter. (B) XRD patterns of 3DP Al_2O_3 objects after sinter using (a)AO/TEOA/Al_2O_3 and (b)AO/TEOA/Al_2O_3/GO inks. (C) Raman spectrum of 3DP Al_2O_3 objects based on AO/TEOA/Al_2O_3/GO. (D) Bending stress-strain curves of the 3DP Al_2O_3 objects using Al_2O_3 inks.

4. Conclusions

In summary, a AO/TEOA gel based on supra-molecular system was developed, which had good compatibility with various organic/inorganic precursors, such as nature rubbers, silica, polymers (eg. EP and PVDF), ceramic (eg. Al_2O_3), metal (eg. Al and CI) and carbon (eg. graphene) etc. In addition, the present gel system also displayed excellent printability that was excellent shear-thinning effect and good shape fidelity, facilitating the successful DIW 3DP processes. The resulting 3D structures exhibited record high solid contents and realize various functions that could not be obtained with conventional ink materials. This study therefore addresses the problem of the lack of suitable DIW inks in various applications.

Acknowledgements

The authors are grateful for the support of the National Natural Science Foundation of China under grants (51773184 and U1810114), Shanxi Provincial Natural Science Foundation of China (201803D421081 and 20181102014).

Conflict of interest

The authors declared that they have no conflicts of interest to this work.

References

[1] Oh Yosep, Witherell Paul, Lu Yan, Sprock Timothy, Nesting and scheduling problems for additive manufacturing: A taxonomy and review. *Additive Manufacturing* 36, 108258 (**2020**).

[2] Barui Srimanta, Ding Hui, Wang Zixin, Zhao Hu, Marathe Shashidhara, Mirihanage Wajira, Basu Bikramjit, Derby Brian, Probing Ink-Powder Interactions during 3D Binder Jet Printing Using Time-Resolved X-ray Imaging. *Acs Applied Materials & Interfaces* 12, 34254-34264 (**2020**).

[3] Yuk Hyunwoo, Lu Baoyang, Lin Shen, Qu Kai, Xu Jingkun, Luo Jianhong, Zhao Xuanhe, 3D printing of conducting polymers. *Nature Communications* 11,1604 (**2020**).

[4] Scott Philip J, Meenakshisundaram Viswanath, Hegde Maruti, Kasprzak Christopher R, Winkler Christopher R, Feller Keyton D, Williams Christopher B, Long Timothy E, 3D Printing Latex: A Route to Complex Geometries of High Molecular Weight Polymers. *Acs Applied Materials & Interfaces* 12, 10918-10928 (**2020**).

[5] Hupfeld Tim, Wegner Andreas, Blanke Meik, Donate-Buendia Carlos, Sharov Vladyslav, Nieskens Simon, Piechotta Markus, Giese Michael, Barcikowski Stephan, Gokce Bilal, Plasmonic Seasoning: Giving Color to Desktop Laser 3D Printed Polymers by Highly Dispersed Nanoparticles. *Advanced Optical Materials* 8, 2000473 (**2020**).

[6] Regehly Martin, Garmshausen Yves, Reuter Marcus, Konig Niklas F, Israel Eric, Kelly Damien P, Chou Chun-Yu, Koch Klaas, Asfari Baraa, Hecht Stefan, Xolography for linear volumetric 3D printing. *Nature* 588, 620-+ (**2020**).

[7] Bhatt Prahar M, Kabir Ariyan M, Peralta Max, Bruck Hugh A, Gupta Satyandra K, A robotic cell for performing sheet lamination-based additive manufacturing. *Additive Manufacturing* 27, 278-289 (**2019**).

[8] Jing Jingjing, Xiong Yu, Shi Shaohong, Pei Haoran, Chen Yinghong, Lambin Philippe,Facile fabrication of lightweight porous FDM-Printed polyethylene/graphene nanocomposites with enhanced interfacial strength for electromagnetic interference shielding. *Composites Science And Technology* 207, 108732 (**2021**).

[9] Li Mengya, Jiang Junjie, Hu Bin, Zhai Wentao, Fused deposition modeling of hierarchical porous polyetherimide assisted by an in-situ CO2 foaming technology. *Composites Science And Technology* 200, 108454 (**2020**).

[10] Talley Samantha J, Branch Brittany, Welch Cynthia F, Park Chi Hoon, Watt John, Kuettner Lindsey, Patterson Brian, Dattelbaum Dana M, Lee Kwan-Soo, Impact of filler composition on mechanical and dynamic response of 3-D printed silicone-based

nanocomposite elastomers. *Composites Science And Technology* 198, 108258 (**2020**).
[11] Zhu Junzhe, Zhang Qiang, Yang Tianqing, Liu Yu, Liu Ren, 3D printing of multi-scalable structures via high penetration near-infrared photopolymerization. *Nature Communications* 11, (**2020**).
[12] Revelo Carlos F, Colorado Henry A, 3D printing of kaolinite clay ceramics using the Direct Ink Writing (DIW) technique. *Ceramics International* 44, 5673-5682 (**2018**).
[13] Gu Shaohua, Tian Yaling, Liang Kai, Ji Yali, Chitin nanocrystals assisted 3D printing of polycitrate thermoset bioelastomers. *Carbohydrate Polymers* 256,117549 (**2021**).
[14] Zhou Luyu, Fu Jianzhong, Gao Qing, Zhao Peng, He Yong, All-Printed Flexible and Stretchable Electronics with Pressing or Freezing Activatable Liquid-Metal-Silicone Inks. *Advanced Functional Materials* 30, 1906683 (**2020**).
[15] Guo Zhiyang, Yu Peishi, Liu Yu, Zhao Junhua, High-precision resistance strain sensors of multilayer composite structure via direct ink writing: Optimized layer flatness and interfacial strength. *Composites Science And Technology* 201,108530 (**2021**).
[16] Hausmann Michael K, Ruhs Patrick A, Siqueira Gilberto, Lauger Jorg, Libanori Rafael, Zimmermann Tanja, Studart Andre R, Dynamics of Cellulose Nanocrystal Alignment during 3D Printing. *Acs Nano* 12, 6926-6937 (**2018**).
[17] Zhou Luyu, Gao Qing, Fu Jianzhong, Chen Qianyong, Zhu Jiapei, Sun Yuan, He Yong, Multimaterial 3D Printing of Highly Stretchable Silicone Elastomers. *Acs Applied Materials & Interfaces* 11, 23573-23583 (**2019**).
[18] Reiser Alain, Linden Marcus, Rohner Patrik, Marchand Adrien, Galinski Henning, Sologubenko Alla S, Wheeler Jeffrey M, Zenobi Renato, Poulikakos Dimos, Spolenak Ralph, Multi-metal electrohydrodynamic redox 3D printing at the submicron scale. *Nature Communications* 10, 1853 (**2019**).
[19] Ajdary Rubina, Huan Siqi, Ezazi Nazanin Zanjanizadeh, Xiang Wenchao, Grande Rafael, Santos Helder A, Rojas Orlando J, Acetylated Nanocellulose for Single-Component Bioinks and Cell Proliferation on 3D-Printed Scaffolds. *Biomacromolecules* 20, 2770-2778 (**2019**).
[20] Imran Muhammad, Ijaz Palvasha, Goldoni Luca, Maggioni Daniela, Petralanda Urko, Prato Mirko, Almeida Guilherme, Infante Ivan, Manna Liberato, Simultaneous Cationic and Anionic Ligand Exchange For Colloidally Stable CsPbBr3 Nanocrystals. *Acs Energy Letters* 4, 819-824 (**2019**).
[21] Xu Yong, Chen Lei, Ye Xingchen, Wang Xuchun, Yu Jiaq, Zhao Yang, Cao Muhan, Xia Zhouhui, Sun Baoquan, Zhang Qiao, Cooperative interactions among CTA(+), Br- and Ag+ during seeded growth of gold nanorods. *Nano Research* 10, 2146-2155 (**2017**).

[22] Mu Liwen, Shi Yijun, Ji Tuo, Chen Long, Yuan Ruixia, Wang Huaiyuan, Zhu Jiahua, Ionic Grease Lubricants: Protic Triethanolamine Oleic Acid and Aprotic Choline Oleic Acid. *Acs Applied Materials & Interfaces* 8, 4977-4984 (**2016**).

[23] Wychowaniec Jacek K, Iliut Maria, Borek Bartłomiej, Muryn Christopher, Mykhaylyk Oleksandr O, Edmondson Steve, Vijayaraghavan Aravind, Elastic flow instabilities and macroscopic textures in graphene oxide lyotropic liquid crystals. *Npj 2d Materials And Applications* 5, (**2021**).

[24] Chandrasekaran Swetha, Yao Bin, Liu Tianyu, Xiao Wang, Song Yu, Qian Fang, Zhu Cheng, Duoss Eric B, Spadaccini Christopher M, Li Yat, Worsley Marcus A, Direct ink writing of organic and carbon aerogels. *Materials Horizons* 5, 1166-1175 (**2018**).

[25] Huan Siqi, Ajdary Rubina, Bai Long, Klar Ville, Rojas Orlando J, Low Solids Emulsion Gels Based on Nanocellulose for 3D-Printing. *Biomacromolecules* 20, 635-644 (**2019**).

[26] Li Vincent C F., Mulyadi Arie, Dunn Conner K, Deng Yulin, Qi H. Jerry, Direct Ink Write 3D Printed Cellulose Nanofiber Aerogel Structures with Highly Deformable, Shape Recoverable, and Functionalizable Properties. *Acs Sustainable Chemistry & Engineering* 6, 2011-2022 (**2018**).

[27] Zhang Hua, Cong Yang, Osi Amarachi Rosemary, Zhou Yang, Huang Fangcheng, Zaccaria Remo P, Chen Jing, Wang Rong, Fu Jun, Direct 3D Printed Biomimetic Scaffolds Based on Hydrogel Microparticles for Cell Spheroid Growth. *Advanced Functional Materials* 30, 1910573 (**2020**).

[28] Zheng Qi, Yu Meijie, Wang Wen, Wang Yanjun, Zhang Ze, Zhou Haiping, Dai Youyong, Wang Chengguo, Xu Yong, Enhanced microwave absorption performance of Fe/C nanofibers by adjusting the magnetic particle size using different electrospinning solvents. *Ceramics International* 46, 28603-28612 (**2020**).

[29] Xie BinGen, Wang Heng, Lu RongLi, Wang Hao, Xia Ru, Chen Peng, Qian JiaSheng, A combined simulation and experiment study on polyisoprene rubber composites. *Composites Science And Technology* 200, 108398 (**2020**).

[30] Ni Yufeng, Yang Dan, Wei Qungui, Yu Liyuan, Ai Jia, Zhang Liqun, Plasticizer-induced enhanced electromechanical performance of natural rubber dielectric elastomer composites. *Composites Science And Technology* 195, 108202 (**2020**).

[31] Xiang Hongping, Yin Jingfeng, Lin Guanghong, Liu Xiaoxuan, Rong Minzhi, Zhang Mingqiu,Photo-crosslinkable, self-healable and reprocessable rubbers. *Chemical Engineering Journal* 358, 878-890 (**2019**).

[32] Li Jingchao, Zhao Xiuying, Wu Wenjie, Zhang Zhaoxu, Xian Yue, Lin Yutao, Lu Yonglai,

Zhang Liqun, Advanced flexible rGO-BN natural rubber films with high thermal conductivity for improved thermal management capability. *Carbon* 162, 46-55 (**2020**).

[33] Chen Qiyi, ZhaoJiayu, Ren Jingbo, Rong Lihan, Cao Peng-Fei, Advincula Rigoberto C, 3D Printed Multifunctional, Hyperelastic Silicone Rubber Foam. *Advanced Functional Materials* 29, 1900469 (**2019**).

[34] Kim WonJin, Kim Minseong, Kim Geun Hyung, 3D-Printed Biomimetic Scaffold Simulating Microfibril Muscle Structure. *Advanced Functional Materials* 28, 1800405 (**2018**).

[35] Park Tae Yoon, Yang Yun Jung, Ha DongHeon, Cho DongWoo, Cha Hyung Joon, Marine-derived natural polymer-based bioprinting ink for biocompatible, durable, and controllable 3D constructs. *Biofabrication* 11, 035001 (**2019**).

[36] Hamidi Armita, Tadesse Yonas, 3D printing of very soft elastomer and sacrificial carbohydrate glass/elastomer structures for robotic applications. *Materials & Design* 187, 108324 (**2020**).

[37] Zhou Yang, Wan Changjin, Yang Yongsheng, Yang Hui, Wang Shancheng, Dai Zhendong, Ji Keju, Jiang Hui, Chen Xiaodong, Long Yi, Highly Stretchable, Elastic, and Ionic Conductive Hydrogel for Artificial Soft Electronics. *Advanced Functional Materials* 29, 1806220 (**2019**).

[38] Li Xuefeng, Wang Hui, Li Dapeng, Long Shijun, Zhang Gaowen, Wu Zi Liang, Dual Ionically Cross-linked Double-Network Hydrogels with High Strength, Toughness, Swelling Resistance, and Improved 3D Printing Processability. *Acs Applied Materials & Interfaces* 10, 31198-31207 (**2018**).

[39] Qu Peiyao, Lv Chi, Qi Yuhao, Bai Lu, Zheng Junping, A Highly Stretchable, Self-Healing Elastomer with Rate Sensing Capability Based on a Dynamic Dual Network. *Acs Applied Materials & Interfaces* 13, 9043-9052 (**2021**).

[40] Davoodi Elham, Montazerian Hossein, Khademhosseini Ali, Toyserkani Ehsan, Sacrificial 3D printing of shrinkable silicone elastomers for enhanced feature resolution in flexible tissue scaffolds. *Acta Biomaterialia* 117, 261-272 (**2020**).

[41] Kozak Nataly, Matzui Lyudmila, Vovchenko Lyudmila, Kosyanchuk Lyudmila, Oliynyk Victor, Antonenko Oksana, Nesin Stanislav, Gagolkina Zoja, Influence of coordination complexes of transition metals on EMI-shielding properties and permeability of polymer blend/carbon nanotube/nickel composites. *Composites Science And Technology* 200, 108420 (**2020**).

[42] Cao Xueyuan, Zhang Juan, Chen Siwei, Varley Russell John, Pan Kai, 1D/2D

Nanomaterials Synergistic, Compressible, and Response Rapidly 3D Graphene Aerogel for Piezoresistive Sensor. *Advanced Functional Materials* 30, 2003618 (**2020**).

[43] Wang Lin, Zhang Meiyun, Yang Bin, Tan Jiaojun, Ding Xueyao, Highly Compressible, Thermally Stable, Light-Weight, and Robust Aramid Nanofibers/Ti3AlC2 MXene Composite Aerogel for Sensitive Pressure Sensor. *Acs Nano* 14, 10633-10647 (**2020**).

[44] Ye Yuhang, Zhang Yifan, Chen Yuan, Han Xiaoshuai, Jiang Feng, Cellulose Nanofibrils Enhanced, Strong, Stretchable, Freezing-Tolerant Ionic Conductive Organohydrogel for Multi-Functional Sensors. *Advanced Functional Materials* 30, 2003430 (**2020**).

[45] Mahapatra A, Mishra B G, Hota G, Synthesis of ultra-fine alpha-Al2O3 fibers via electrospinning method. *Ceramics International* 37, 2329-2333 (**2011**).

[46] Li Ziyan, Fu Lvping, Gu Huazhi, Or Siu Wing, Huang Ao, Lv Renxiang, Fabrication of in-situ Ti(C,N) phase toughened Al2O3 based ceramics from natural bauxite. *Ceramics International* 47, 25497-25504 (**2021**).

[47] Yang Liangliang, Zeng Xiaojun, Ditta Allah, Feng Bo, Su Lizhong, Zhang Yue, Preliminary 3D printing of large inclined-shaped alumina ceramic parts by direct ink writing. *Journal Of Advanced Ceramics* 9, 312-319 (**2020**).